

Optical field simulation of edge coupled terahertz quantum well photodetectors

Lujia Li,^{1,2} Peng Bai,^{1,2} Yueheng Zhang,^{1,2,a} Wenzhong Shen,^{1,2}
and Juncheng Cao³

¹Key Laboratory of Artificial Structures and Quantum Control, Department of Physics
and Astronomy, Shanghai Jiao Tong University, Shanghai 200240, China

²Collaborative Innovation Center of Advanced Microstructures, Nanjing 210093, China

³Key Laboratory of Terahertz Solid-State Technology, Shanghai Institute of Microsystem
and Information Technology, Chinese Academy of Sciences, Shanghai 200050, China

(Received 3 November 2017; accepted 6 March 2018; published online 19 March 2018)

By finite difference time domain (FDTD) simulation, we report on the optical field distribution within edge coupled terahertz quantum well photodetectors (THz QWPs) in detail. The coupling efficiency of THz QWP structures are studied from three aspects, including the electrode geometry, the position of the active region and the coupling angle. According to the simulation results, proper electrode geometry is suggested in different frequency region, and the optimal position of active region and coupling angle are presented. These results provide a useful guidance for the design and fabrication of the edge coupled THz QWP. © 2018 Author(s). All article content, except where otherwise noted, is licensed under a Creative Commons Attribution (CC BY) license (<http://creativecommons.org/licenses/by/4.0/>). <https://doi.org/10.1063/1.5011956>

I. INTRODUCTION

Due to the rapid development of terahertz science and technology, terahertz quantum well photodetectors (THz QWPs) have attracted more and more attention nowadays because of some unique advantages such as fast intrinsic response speed, wide wavelength coverage and the availability of a mature material and processing.^{1,2} Though assumed to be a natural extension of the traditional infrared (IR) QWPs to the THz frequency, the study on THz QWP is far from mature. At present, the primary goal of THz QWP investigation still remains to be improving the device performance as possible. Therefore, a lot of studies have been devoted to the device optimization. The device parameters, including the quantum well width, the aluminum fraction, the doping concentration and the quantum well number, are chosen to have the highest sensitivity and operating temperature.²⁻⁶

It is known that optical field distribution within the detector is another key factor affecting the performance.^{1,7} Helm⁷ pointed out that the intersubband absorption with a small number of QW periods located near the surface could be enhanced by a metal coating. H. Schneider et al.⁸ showed that the optical excitation within the active region of a mid-infrared QWIP was inhomogeneous and influenced the QWIP responsivity and its voltage dependence. The inhomogeneity can be suppressed by using mesa photodetectors where only half of the top contact is covered with metal.⁸ By simulating the optical field of edge coupled IR QWPs, K. K. Choi pointed out that the 45° coupling angle is not the best one.⁹ To obtain better performance, realization of the optical field distribution is necessary in addition to the conventional optimization of the detector parameters.

In contrast to traditional IR QWPs, the wavelength of THz radiation is comparable to the device size of THz QWPs and much longer than the length scale of its active region, where the influence of optical field distribution is more significant. For THz QWP, the grating¹⁰⁻¹⁶ and antenna¹⁶⁻²⁰ designs

^aElectronic mail: yuehzhang@sjtu.edu.cn

have been carried out to obtain high absorption by adjusting the optical field inside the device. However, relevant studies on optical field distribution for THz QWP are still limited up to now. The detailed investigation on optical field distribution of the edge coupled THz QWPs has hardly been elaborated before. According to the intersubband transition (ISBT) selection rule of QWPs, only light polarized in epitaxial growth direction leads to the absorption. Therefore, 45° edge coupled geometry is commonly employed to obtain a detector performance.¹ The realization of the actual optical field distribution inside an edge coupled THz QWP is essentially needed and important for device optimization.

In addition, 45° facet coupled THz QWP is usually looked upon as a benchmark. To evaluate the performance of THz QWPs, different 45° facet coupled THz QWPs are compared with each other experimentally. And THz QWPs with optical cavity design, e.g. grating or antenna, are usually compared with 45° facet coupled THz QWP. However, due to the significant effect of electrode geometry on the optical field distribution, whether the comparison between different devices is meaningful arises to be a question and need to be studied carefully.

In this paper, we systematically simulate the optical field distribution of the edge coupled THz QWP in the entire THz radiation range theoretically by applying finite difference time domain (FDTD) modeling method. There are two electrode geometries (solid and ring) that is widely used in practical application of the edge coupled THz QWPs. So we first discuss the optical field distribution and coupling efficiency of two different electrode geometries in the THz range, which gives a guidance of the electrode geometry application for the edge coupled THz QWPs. Then we study the effect of the location of active region on the performance of THz QWPs and give the best location of the active region for THz QWPs operating at different peak frequencies. Finally, we investigate the effect of coupling angle and reveal the appropriate coupling angle at different frequency.

II. THEORETICAL MODEL AND METHOD

The finite difference time domain (FDTD) technique is used to simulate the optical field distribution in multilayer structures of THz QWPs. A schematic view of a random α angle edge coupled THz QWP for simulation is shown in Fig. 1(a). This figure is not drawn to scale. The structure is composed of a top contact layer, multiple periods of GaAs/AlGaAs quantum well (MQW) active region, a bottom contact layer and the semi-insulating GaAs substrate. Au electrode is covered on the top and bottom contact layer. For the top Au electrode, either solid or ring geometry could be used in terms of practical need. The solid electrode means that the mesa is completely covered by a metal coating. Therefore, the size of the solid electrode is exactly as that of the mesa. As far as the ring electrode is concerned, we presume that it is very narrow compared with the size of mesa and the width is ignored in the simulation. The terahertz radiation light is shone normal to the edge facet. In order to simulate the spatial distribution of the optical excitation density along the growth axis, we assume that a light beam is incident on a facet with a wave vector \vec{k} at an angle α with respect to the growth direction. The optical field distribution in direction perpendicular to the plane of incidence is invariant. Hence, a 2-dimensional model is employed in the simulation. The coordinates and the origin of the coordinates are labeled in the figure. $y=0$ denote the semiconductor-top metal interface. Due to the fact that only light polarized in y direction leads to the absorption, only y component of electromagnetic wave is concerned.

The prototype of THz QWP studied here is v266 from Ref. 21. The thickness is 0.5 μm , 0.4 μm , 2.6 μm and 0.8 μm for the Au electrode layer, top contact layer, MQW active region and the bottom contact layer, respectively. The semi-insulating substrate thickness is usually in the range of 600 μm . The area of the mesa devices is set to be 400 \times 400 μm^2 . It should be noted that the free-carrier absorption is relatively strong in terahertz region. In order to reduce the free-carrier absorption and plasma reflection of the contact layer, the doping concentration in the contact layer is usually designed to a relatively low level. Actually, the usual doping concentration is designed to be merely on the order of $\sim 1 \times 10^{17}$ cm^{-3} in terahertz region.^{21,22} For simplicity, the GaAs/AlGaAs MQW layer is replaced by a uniform intrinsic GaAs layer because of the low doping density and Al fraction in the calculation.

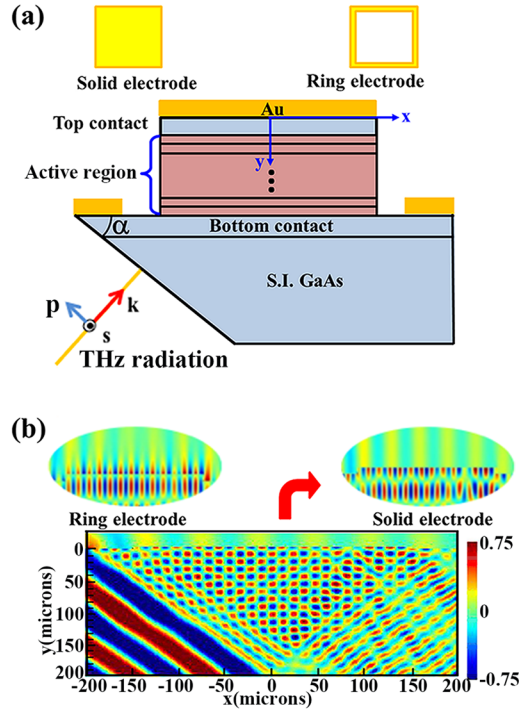


FIG. 1. (a) Schematic view of a random α angle edge coupled THz QWP. The figure is not drawn to scale. (b) E_y pattern in the device of the simulated 45° edge coupled QWP with solid electrode geometry. The peak frequency is at 5THz. The arrow indicates the local optical field distribution around the mesa for solid electrode. As a contrast, the corresponding pattern in ring electrode case is shown on the left side.

The dielectric functions $\varepsilon(\omega)$ of GaAs is calculated in terms of a classical dielectric function for damped harmonic oscillators in combination with a Drude model:¹²

$$\varepsilon(\omega) = \varepsilon_\infty \left[1 - \frac{\omega_p^2}{\omega(\omega + i\omega_0)} \right] + \frac{\omega_{TO}^2(\varepsilon_s - \varepsilon_\infty)}{\omega_{TO}^2 - \omega^2 - i\omega\gamma}. \quad (1)$$

The first term in the right describes the free carrier absorption.²³ $\omega_p = \sqrt{N_d q^2 / \varepsilon_0 \varepsilon_s m_e^*}$ is the plasma frequency. The second term is the Reststrahlen term, which describes the interaction with optical phonons.²³ ω_{TO} is the transverse optical (TO) phonon frequency. The related parameters are taken from Ref. 23. The dielectric function of metal electrode is calculated by the Drude model:¹²

$$\varepsilon_M(\omega) = 1 - \frac{\omega_M^2}{\omega(\omega + i\delta_M)}, \quad (2)$$

in the case of gold, $\omega_M = 1.11 \times 10^4$ THz and $\delta_M = 83.3$ ps⁻¹.

Perfectly Matched Layers (PML) absorbing boundary conditions is applied.²⁴ Due to the fact that the doping concentration is usually low for THz QWP, the absorption is merely proportional to the period number of wells.¹ It's not necessary to take into account the difference between the active region absorption at different THz frequency. Therefore, the absorption efficiency is proportional to the coupling efficiency of the THz QWP. The average intensity of E_y in the active region could be looked upon as a measure of the optical coupling efficiency. We define a normalized coupling efficiency η to be:

$$\eta = \frac{\iint_{S_{AR}} |E_y|^2 dS}{\iint_{S_{AR}} |E_{y0}|^2 dS}, \quad (3)$$

where S_{AR} is the area of the active region, E_{y0} is the y component of incident electrical field.

E_y pattern in the entire THz QWP could give an intuitive view of the electrical field spatial distribution. We first present an example of E_y pattern for a THz QWP with solid electrode geometry at 5THz in Fig. 1(b). The E_y pattern shows that the device forms a cavity with two parallel partial reflectors. Interference between the incident and reflected radiation gives rise to standing wave effects. Local maxima and minima can be seen clearly. The optical field spatial distribution varies obviously because of different electrode geometry. The arrow indicates the local optical field distribution around the mesa for solid electrode. As a contrast, the corresponding pattern in ring electrode case is shown on the left side. It is obvious that the optical field in the active region for the solid electrode is relatively strong, which means a higher coupling efficiency. In the case of ring electrode, the optical field above the top surface is strong where an evanescent field exists. The totally reflection critical angle of GaAs is about 17.6° . When the light is incident at 45° angle, it is totally reflected at semiconductor-air interface of the top surface. Thereby, there is no refraction light but an evanescent field. The evanescent field propagates along the semiconductor-air interface. And the amplitude decreases exponentially at direction perpendicular to the interface.

Up to now, THz QWPs that are studied experimentally before mainly operate in a range of 3.2 THz to 11.37 THz.^{21,22,25,26} To study the characteristic of THz QWPs in low, medium and high THz frequency region, we take 2 THz, 6.5 THz and 12THz as three typical THz frequencies in the following calculation.

III. NUMERICAL RESULTS AND DISCUSSION

A. The effect of electrode geometry

Previous studies show that the electrode geometry affects the optical excitation and thereby influences the absorption in mid-infrared.⁸ To figure out the case in THz range, we consider two different types of electrode geometry, the solid and ring electrode. The $|E_y|$ patterns within the active region of 45° edge coupled QWP with solid and ring electrode at 2 THz, 6.5 THz, and 12 THz are presented in Figs. 2(a)–2(f). It is clear that the electrode geometry affects the optical field distribution apparently. For the low THz frequency, e.g. 2 THz, $|E_y|$ in THz QWP with solid electrode is much stronger than that with ring electrode, as shown in Figs. 2(a) and 2(d). This means that solid electrode geometry is more suitable in low THz frequency. In contrast, for high frequency, such as 12 THz as shown in Figs. 2(c) and 2(f), $|E_y|$ intensity in THz QWP with ring electrode case is relatively large compared with the case of solid electrode. And for the medium frequency of 6.5 THz, the average intensity of E_y in the total active region area is comparable for such two different electrode geometries, but the intensity of $|E_y|$ at local position is different, as displayed in Figs. 2(b) and 2(e). Therefore, to obtain a high coupling efficiency, the active region should be located at some certain positions, which will be discussed in detail in the following section.

In order to determine the effect of electrode geometry, we calculate the coupling efficiency η of 45° edge coupled QWP from 1 THz to 12 THz. We first simulate the coupling efficiency of without considering doping in contact layer, as shown in Fig. 2(g). Based on the practically applied THz QWP structures (v266 in Ref. 1), the influence of different electrode geometry is demonstrate quantitatively. It is seen that the entire THz radiation range could be divided into three zones, the low frequency zone (1-6.7 THz), the medium frequency zone (6.7-9.8 THz) and the high frequency zone (9.8-12 THz). In low frequency region, the coupling efficiency η with solid electrode is always higher than that with ring electrode. This effect gets more and more obvious as the frequency decreasing. Due to the half-wave loss in solid electrode case, the intensity of interference light near the semiconductor-metal interface (where the MQW active region locates) is relatively strong. In low frequency region, the total thickness of MQW active region is much shorter compared to the wavelength of interference light, which means the MQW active region could wholly locates at the local maxima position. At 1 THz, the coupling efficiency for THz QWP with solid electrode is about 24 times higher than that with ring electrode, indicating the device performance would be sacrificed greatly if a ring electrode is applied improperly. In contrast, in high frequency region, THz QWP with ring electrode shows superiority. η in this case is about twice as the one with solid electrode at 12 THz. In the medium frequency region, η in both cases is low and comparable to each other because of the influence of the

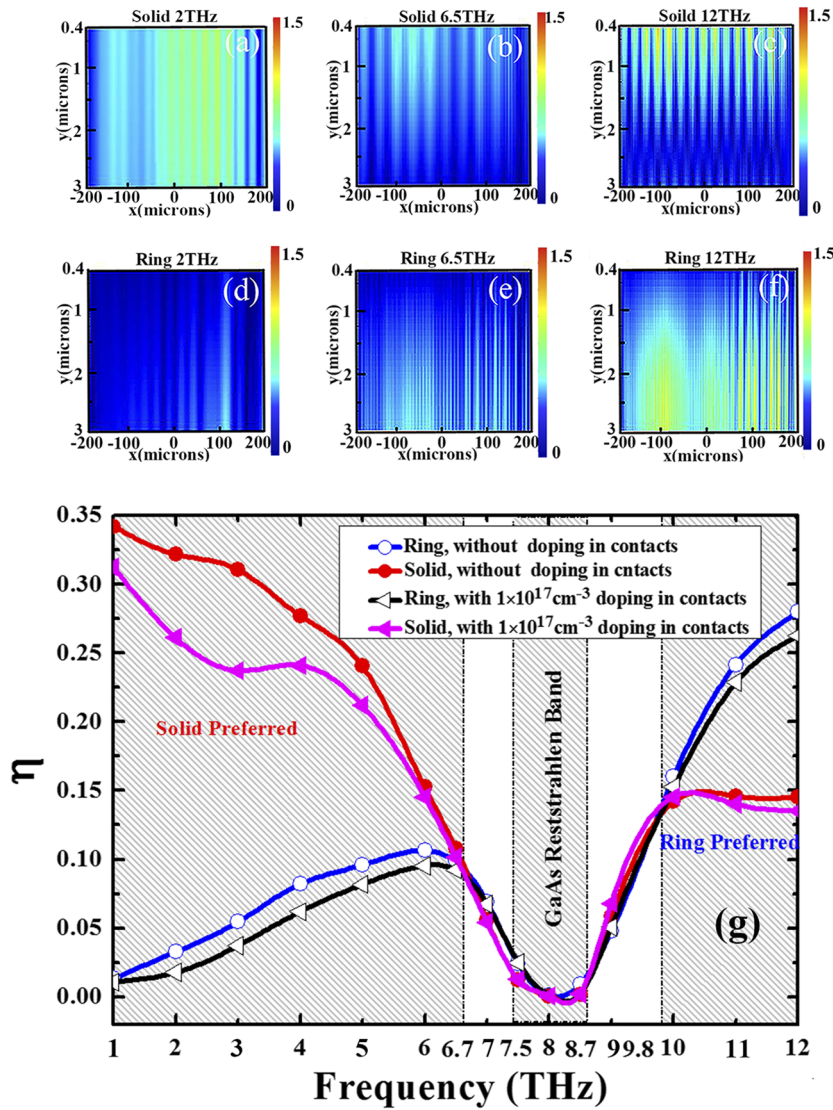


FIG. 2. $|E_y|$ patterns within the active region in the condition of (a) $f=2\text{THz}$, solid electrode, (b) $f=6.5\text{THz}$, solid electrode, (c) $f=12\text{THz}$, solid electrode, (d) $f=2\text{THz}$, ring electrode, (e) $f=6.5\text{THz}$, ring electrode and (f) $f=12\text{THz}$, ring electrode, (g) the coupling efficiency of both kinds of QWP structure condition (without considering doping in contact layer and with $1 \times 10^{17} \text{ cm}^{-3}$ doping in contact layers) in 1-12 THz region.

GaAs Reststrahlen band (7.5 - 8.7 THz).²⁷ In this frequency region, the radiation electromagnetic wave and lattices vibrating of transverse optical mode couple with each other strongly, so that the reflectivity could be nearly 100%. The high reflectivity results in the low coupling efficiency. The discussion is in accordance with the real situation and could provide a guidance of the electrode geometry selection for the edge coupled THz QWPs.

It should be noted that the free-carrier absorption could have an influence on the optical field in the active region. In fact, this affecting factor has already been taken into consideration in the practical design of THz QWP. In order to reduce the free-carrier absorption and plasma reflection of the contact layer, the doping concentration is usually designed to a relatively low level. Actually, the usual doping level in the contact layer is designed to be merely on the order of $\sim 1 \times 10^{17} \text{ cm}^{-3}$ in terahertz region.^{21,22} To evaluate the influence of the doping in contact layer, another simulation was also carried out in which the typical doping concentration of $1 \times 10^{17} \text{ cm}^{-3}$ in contact layers are well considered. The simulation results are also given in Fig. 2(g). The coupling efficiency η is

reduced a little because of the free-carrier absorption in the doped contact layer for both electrode geometries. Nevertheless, the difference of between the two electrode geometries at a given frequency is almost equal as that without considering the doping. Because the resulted difference itself is not obvious and the final conclusion about frequency scope for the suggested electrode geometry is not changed, it is reasonable for us to neglect the effect of the doping in contact layer in the following simulations.

It is known that, the 45° edge coupled device is usually looked upon as a benchmark.¹ To evaluate the performance, different THz QWP are usually needed to compare with each other and 45° edge coupling is the most widely adopted coupling mode. However, according to the above discussion, the electrode geometry may affect the device performance greatly, especially in low frequency region. The performance of a THz QWP is better than another one doesn't necessarily mean a more reasonable device parameter if the effect of the electrode geometry is not considered. In terahertz frequency range, it is necessary to pay attention to the electrode geometry when compared. Different comparison results may be obtained if different electrode geometry is employed for the 45° edge coupled THz QWP. This is also the case for the comparison between the grating (or antenna) designed THz QWP and the 45° edge coupled THz QWP. In most cases, to verify the design superiority of the grating or the antenna structures, the newly designed structures are usually compared with the 45° edge coupled THz QWP, too. But there may exist a misunderstanding or misleading on this issue. As a reference substance, what kind of electrode geometry is applied for the 45° edge coupled THz QWP. The comparison should be based on the best performance values of both newly designed structure and 45° edge coupled structure. However, the performance of conventional 45° edge coupled structure was underestimated in some of the previous studies because improper electrode geometry is used. The THz QWP with ring electrode is obviously not suitable for comparison in low frequency region, which may lead to the benchmark value relatively low. And the results based on such comparison are clearly unreasonable and misleading. To provide a reasonable performance benchmark, a solid electrode should be used in low frequency region and a ring one is preferred in high frequency region. And it is necessary to point out the electrode geometry of the 45° edge coupled THz QWP clearly when compared.

B. The effect of the position of the active region

According to the results of Figs. 2(a)–2(f), local maxima and minima of $|E_y|$ arise due to the interference between incident and reflected infrared light. To get higher coupling efficiency, the active region should be located around the maximum position of $|E_y|$. The typical thickness of active region in THz QWP is around 2.6 μm , which is a much shorter length scale compared with the wavelength of terahertz light. This characteristic implies that the reasonable location of active region is of great significance for high coupling efficiency. And we need to know the spatial distribution of $|E_y|$ in the entire THz QWP.

The spatial distributions of $|E_y|$ within the top 30 μm (including the active region and part of the substrate region) at three typical frequency 2 THz, 6.5 THz and 12 THz are shown in Figs. 3(a)–3(f). No matter what frequency and electrode geometry are, a standing wave of local maxima and minima can be seen clearly. In order to get higher coupling efficiency, the active region should be located around the maximum position of $|E_y|$ by inserting an additional spacer between the electrode and the active region. In the case of solid electrode, the first maximum positions of $|E_y|$ for 2 THz, 6.5 THz and 12 THz QWP are right at $y=0 \mu\text{m}$, as shown in Figs. 3(a)–3(c). In contrast, in the case of the ring electrode, as presented in Figs. 3(d)–3(f), the first maximum positions of $|E_y|$ are away from the top surface and locate at $y=16 \mu\text{m}$, $y=5 \mu\text{m}$, $y=2.7 \mu\text{m}$ below the top surface for 2 THz, 6.5 THz and 12 THz QWP respectively. Therefore, the thickness of the spacer is dependent on the frequency of incident light. The lower the frequency is, the thicker the spacer is.

To obtain an intuitive view of the location of active region center and the corresponding thickness of the spacer, the spatial distribution of the optical excitation density along the growth axis in the case of both kinds of electrode are estimated in terms of Ref. 8. For the solid electrode geometry,

$$\vec{E} = \begin{pmatrix} E_x \\ E_y \end{pmatrix} = 2E \exp(ik_x x - i\omega t) \begin{pmatrix} i \cos \alpha \sin(k_y y) \\ \sin \alpha \cos(k_y y) \end{pmatrix}. \quad (4)$$

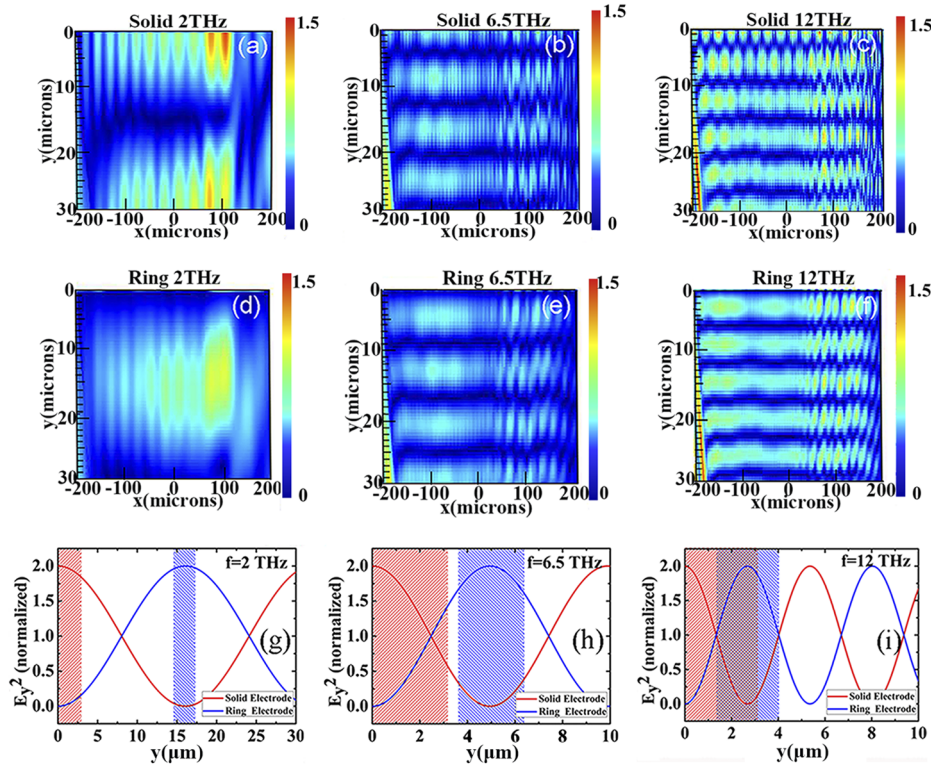


FIG. 3. (a-f) $|E_y|$ patterns in the top 30 μm ($y=0$ denote the semiconductor-top metal interface), respectively for (a) $f=2$ THz, solid electrode, (b) $f=6.5$ THz, solid electrode, (c) $f=12$ THz, solid electrode, (d) $f=2$ THz, ring electrode, (e) $f=6.5$ THz, ring electrode, and (f) $f=12$ THz, ring electrode, (g-i) spatial dependence of E_y^2 in ring electrode (blue line) case and solid electrode (red line) case. The frequency of incident terahertz light is (g) 2 THz, (h) 6.5 THz, and (i) 12 THz, respectively. The shadows indicate the optimal active region position. The optimal position of the active region should be located at where the optical excitation is the strongest, i.e. the peak of E_y^2 .

When the ring electrode is applied,

$$\vec{E} = \begin{pmatrix} E_x \\ E_y \end{pmatrix} = 2E \exp(ik_x x - i\omega t) \begin{pmatrix} \cos \alpha \cos(k_y y) \\ i \sin \alpha \sin(k_y y) \end{pmatrix}, \quad (5)$$

in the case of total reflection. Here, \vec{E} is the electric field, \vec{k} is the wave vector, $k_x = |\vec{k}| \sin \alpha$, $k_y = |\vec{k}| \cos \alpha$, α is the angle between \vec{k} and the growth direction. Figs. 3(g)–3(i) display the optical excitation density along the growth axis for solid and ring electrode geometry in terms of Eq. (2) and (3) at 2 THz, 6.5 THz and 12 THz. The optical excitation density is strongest at the peak position. To obtain the high coupling efficiency, the active region should be located at the peak position. In the figure, the active region is demonstrated in shadow. It is obvious that in the low THz frequency, e.g. 2 THz, the length scale of the active region is much smaller than that of the wavelength. Therefore, the location of the active region will affect the coupling efficiency (and also the responsivity) of the device significantly. Taking 2 THz QWP with a solid electrode as an example, if the active region is centered at 8.1 μm (correspondingly the thickness of the spacer is 6.8 μm), the absorption will be 50% of the peak absorption. As the wavelength decreasing (frequency increasing), such as in the medium and high frequency, length scale of the active region is comparable to that of the wavelength. The effect of the active region location is not as sensitive as that at low frequency. Figs. 3(g)–3(i) show that the calculation results corresponding to the first maximum interference position based on optical interference theory are well consistent with the results calculated by FDTD. Figs. 3(i) also well explains why a ring electrode is preferred above phonon band in Section A. For normally applied 45° edge coupled THz QWP discussed, the actual active region locates from $y=0.4$ to $y=3.0$ μm .

In this region, the optical excitation density for the ring electrode is higher than that for the solid electrode, resulting in a high coupling efficiency.

The optimal central position of active region for 45° edge coupled THz QWPs at different frequency is shown in Fig. 4. According to the simulation results of Fig. 3, if a solid electrode is applied, the active region should always be located at $y=0 \mu\text{m}$. However, considering the thickness of the active region, the optimal center position of active region is displayed in red line for solid electrode geometry. In the case of the ring electrode geometry, the optimal central position of the active region is far away from the top surface as the frequency decreasing. In fact, for an actual THz QWPs, it is not practical to use a very thick top contact layer considering the requirement of fabrication. Therefore, the optimal position only provides a guidance to approach. The actual central position of samples v265, v266, v267, L924, and L925 proposed in Ref. 21 and Ref. 22 are also given in Fig. 4. Samples v265 and v266 were designed with top ring electrode, which is labeled by hollow symbols. Samples v267, L924 and L925 was covered by solid electrode, which is labeled by solid symbols. It is clear that the active region is away from the optimized position for samples v265 and v266, indicating that the coupling efficiency can be greatly improved if the central position of active region is changed. For sample v265, the actual position of active region is located at $y=1.7 \mu\text{m}$ while the suggested optimal central position is located at $y=3.4 \mu\text{m}$. The optimized coupling efficiency would be 1.7 times as that of the present one. Similarly, for sample v266, the coupling efficiency would increase 1.7 times if its active region is put in the optimal location. This means that the device performance of sample v265 and v266 were sacrificed greatly because of the improper design of position of active layer.

C. The effect of coupling angle

Generally, the 45° edge facet light-coupling geometry is commonly employed to obtain a detector performance. Though this geometry “throws away” part of the light, it is convenient to realize and usually used to obtain a detector performance benchmark.¹ However, whether 45° is the best coupling angle and the dependence of the incident angle on the coupling efficiency need to be explored. K. K. Choi⁹ studied the effect of the coupling angle on optical coupling efficiency of mid-infrared QWP with a solid electrode. Further investigations on THz QWPs with both solid electrode and ring electrode are needed.

As shown in Fig. 5, we calculate the coupling efficiency at different incident angles. The relation between the coupling efficiency η and the incident angle at three typical frequency 2 THz, 6.5 THz and 12 THz are displayed. It is clear that the coupling efficiency shows obvious angular dependence no matter what kind of electrode geometry is applied.

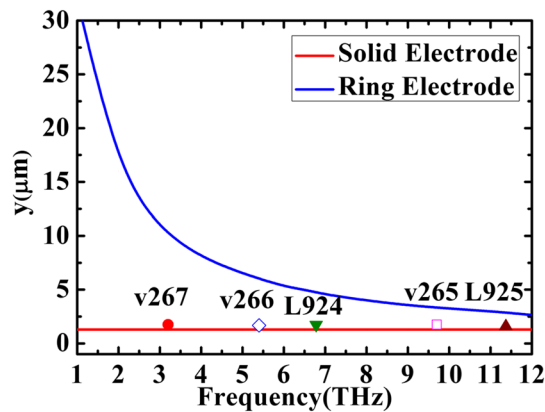


FIG. 4. The dependence of the optimal central position of the active region for 45° edge coupled THz QWPs on frequency. The red and blue lines represent the optimal central position of active region for THz QWPs with solid electrode and ring electrode, respectively. The actual central position of samples v265, v266, v267, L924, and L925 proposed in Ref. 21 and 22 are also given. Samples v265 and v266 were designed with top ring electrode, which is labeled by hollow symbols. Samples v267, L924 and L925 was covered by solid electrode, which is labeled by solid symbols.

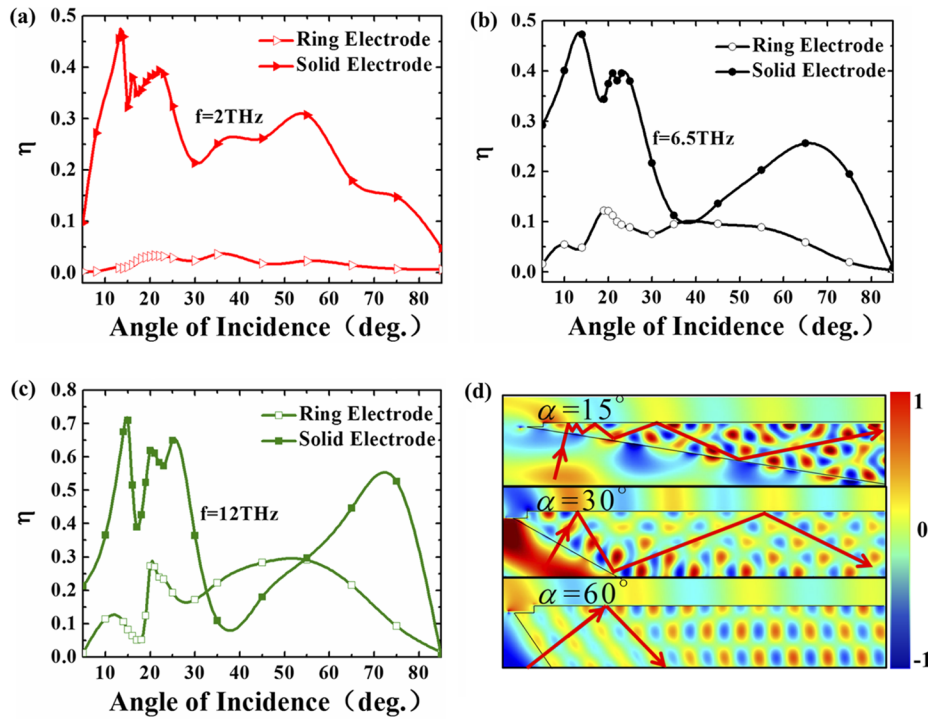


FIG. 5. The relation between the coupling efficiency η and the incident angle for edge coupled THz QWPs with solid and ring electrode geometry at (a) 2 THz, (b) 6.5 THz, and (c) 12 THz. (d) E_y patterns in the vicinity of mesa for 15°, 30° and 60° edge coupled geometry at representative 6.5 THz. The arrows indicate the schematic light paths.

In the case of solid electrode, the coupling efficiency oscillates with the incident angle greatly and 45° is apparently not the best coupling angle. When the angle is reduced, several peaks occur. For example, at 2 THz, the maximum η occurs at 13° and is almost two times as that at 45°. And at 6.5 THz and 12 THz, η also approaches the highest value at around 13°, which agrees well with results of K. K. Choi.⁹ Though the coupling efficiency can be enhanced as the wedge angle decrease, the GaAs substrate will be very thin and fragile, which is unpractical in the view of processing. As the angle increase, the coupling efficiency could also exceed that of 45°. Such effect is more and more obvious as the frequency increasing. At 2 THz, η at 55° is only 25.3 percent higher than η at 45°. In contrast, at 6.5 THz, η at 65° is 88.5% higher than that at 45°. And in the case of 12 THz, η at 75° is three times as that at 45°.

The reason that several peaks (two to three) observed for angles in the range 10° - 30° and the maximum observed at large angle (~70°) could be understood as a waveguide effect⁹ or the interference effect. However, it seems that the interference effect is more appropriate and easy to understand. To present such effect more intuitively, E_y patterns in the vicinity of mesa at three angles are presented as examples in Fig. 5(d). The schematic possible light paths for such three angles are also given in this diagram. It is clear that the light is reflected repeatedly between the semiconductor-metal interface and the grinding facet. Local maximum of the coupling efficiencies could always be obtained at some specific angles where constructive interference condition is satisfied. Therefore, the coupling efficiency oscillates with the angle. In cases of small wedge angles, multiple reflections exist, leading to the constructive interference condition is satisfied more easily. So compared with the case at large angle, more peaks of the coupling efficiency occur.

In the case of the ring electrode, η also depends on the incident angle. Though η can also get the highest value at small angle, the difference between the peak value and the one at 45° is not so significant at these frequencies. Therefore, 45° could be looked upon as a good coupling angle. Compared with the case for the solid electrode, the oscillation with incident angle for the ring electrode fades a lot, especially in small angles. This is because in small angles the refraction occurs and less light reflects in the device, resulting in the constructive interference is reduced. In addition, because

the phase changes compared with the case of the solid electrode, the peak coupling efficiency is found at different angles.

IV. CONCLUSION

We investigate the optical field distribution of edge coupled terahertz quantum well photodetectors by finite difference time domain technique. The optical field dependence of three possible factors, including the electrode geometry, the location of the active region and the coupling angle, was simulated and discussed in detail.

The optical field dependence of electrode geometry is first studied. For normally applied 45° edge coupled QWP, the entire THz radiation range could be divided into three zones, the low frequency zone (1-6.7 THz), the medium frequency zone (6.7-9.8 THz) and the high frequency zone (9.8-12 THz). In low frequency region, the coupling efficiency for the solid electrode geometry is increasingly higher than that for the ring electrode as frequency decreases. Therefore, the solid electrode geometry is preferred in such frequency region. In medium region, both electrode geometries show weak optical coupling efficiency. In high frequency region, ring electrode geometry shows superiority. Due to this reason, it is necessary to point out the electrode geometry of the 45° edge coupled THz QWP clearly when compared. The optimal central position of the active region to obtain a good coupling efficiency is then investigated. In the case of solid electrode, the optimal position of the active region should be right under the top surface ($y=0 \mu\text{m}$). In contrast, in the case of the ring electrode, the optimal position is away from the top surface. The thickness of the spacer is dependent on the frequency of incident light. The lower the frequency is, the thicker the spacer is. Lastly, we studied the dependence of the coupling efficiency on the incident angle. In the case of solid electrode geometry, 45° is apparently not the best angle for optical coupling. η approaches the highest value at around 13° . And as the coupling angle increasing, the coupling efficiency could also exceed that of 45° . Such effect is more and more obvious as the frequency increasing. In the case of the ring electrode, 45° could be looked upon as a good coupling angle.

The discussions on the optical field distribution of edge coupled THz QWPs under different situation provides guidance in designing the THz QWPs.

ACKNOWLEDGMENTS

This work was supported by the Natural Science Foundation of China (91221201) and 863 Program of China (2011AA010205).

- ¹ H. Schneider and H. C. Liu, *Quantum Well Infrared Photodetectors: Physics and Applications* (Springer, 2006).
- ² J. Y. Jia, T. M. Wang, Y. H. Zhang, W. Z. Shen, and H. Schneider, *IEEE T. THz. Sci. Technol.* **5**, 715 (2015).
- ³ S. Zhang, T. M. Wang, M. R. Hao, Y. Yang, Y. H. Zhang, W. Z. Shen, and H. C. Liu, *J. Appl. Phys.* **114**, 194507 (2013).
- ⁴ H. C. Liu, H. Luo, C. Y. Song, Z. R. Wasilewski, A. J. Spring Thorpe, and J. C. Cao, *Infrared Phys. Technol.* **50**, 191 (2007).
- ⁵ H. C. Liu, H. Luo, C. Y. Song, Z. R. Wasilewski, A. J. Spring Thorpe, and J. C. Cao, *IEEE J. Sel. Top. Quant. Electron.* **14**, 374 (2008).
- ⁶ X. G. Guo, J. C. Cao, R. Zhang, Z. Y. Tan, and H. C. Liu, *IEEE J. Sel. Top. Quant. Electron.* **19**, 8500508 (2013).
- ⁷ M. Helm, *The Basic Physics of Intersubband Transitions* (Academic Press, London, 2000).
- ⁸ H. Schneider, C. Schonbein, M. Walther, P. Koidl, and G. Weimann, *Appl. Phys. Lett.* **74**, 16 (1999).
- ⁹ K. K. Choi, *J. Appl. Phys.* **111**, 124507 (2012).
- ¹⁰ L. Stabellini, W. Lu, A. D. Rossi, T. Antoni, M. Carras, S. Trillo, and B. Gaetano, *Opt. Quant. Electron.* **40**, 1085 (2008).
- ¹¹ R. Zhang, X. G. Guo, C. Y. Song, M. Buchanan, Z. R. Wasilewski, J. C. Cao, and H. C. Liu, *IEEE Electron Device L.* **32**, 659 (2011).
- ¹² R. Zhang, X. G. Guo, J. C. Cao, and H. C. Liu, *J. Appl. Phys.* **109**, 073110 (2011).
- ¹³ R. Zhang, Z. L. Fu, L. L. Gu, X. G. Guo, and J. C. Cao, *Appl. Phys. Lett.* **105**, 231123 (2014).
- ¹⁴ J. Y. Ding, X. S. Chen, Q. Li, Y. L. Jing, Z. F. Li, N. Li, and W. Lu, *J. Appl. Phys.* **116**, 083101 (2014).
- ¹⁵ J. Y. Ding, X. S. Chen, Q. Li, W. W. Tang, C. L. Liu, H. L. Zhen, Y. L. Jing, H. Wang, and W. Lu, *Opt. Quant. Electron.* **47**, 2347 (2015).
- ¹⁶ L. Liu, Y. Chen, Z. Huang, W. Du, P. Zhan, and Z. L. Wang, *Sci. Rep.* **6**, 30414 (2016).
- ¹⁷ W. A. Beck and M. S. Mirotznik, *Infrared Phys. Technol.* **42**, 189 (2001).
- ¹⁸ Y. Todorov, A. M. Andrews, I. Sagnes, R. Colombelli, P. Klang, G. Strasser, and C. Sirtori, *Phys. Rev. Lett.* **102**, 186402 (2009).
- ¹⁹ Y. Nga Chen, Y. Todorov, B. Askenazi, A. Vasanelli, G. Biasiol, R. Colombelli, and C. Sirtori, *Appl. Phys. Lett.* **104**, 031113 (2014).

- ²⁰ D. Palaferri, Y. Todorov, Y. N. Chen, J. Madeo, A. Vasnelli, L. H. Li, A. G. Davies, E. H. Linfield, and C. Sirtori, *Appl. Phys. Lett.* **106**, 161102 (2015).
- ²¹ H. Luo, H. C. Liu, C. Y. Song, and Z. R. Wasilewski, *Appl. Phys. Lett.* **86**, 231103 (2005).
- ²² J. Y. Jia, J. H. Gao, M. R. Hao, T. M. Wang, W. Z. Shen, Y. H. Zhang, J. C. Cao, and H. Schneider, *J. Appl. Phys.* **116**, 154501 (2014).
- ²³ G. Yu, Y. H. Zhang, and W. Z. Shen, *Appl. Surf. Sci.* **199**, 160 (2002).
- ²⁴ A. Taflov and S. C. Hagness, *Computational Electromagnetics: The Finite-Difference Time-Domain Method*, 3rd ed (Artech House, Inc., 2005).
- ²⁵ M. Graf, G. Scalari, D. Hofstetter, and J. Faist, *Appl. Phys. Lett.* **84**, 475 (2004).
- ²⁶ H. C. Liu, C. Y. Song, A. J. Springthorpe, and J. C. Cao, *Appl. Phys. Lett.* **84**, 4068 (2004).
- ²⁷ C. Franke, M. Walther, M. Helm, and H. Schneider, *Infrared Phys. Technol.* **70**, 30 (2015).